Structural Characterization and Fluxional Behavior of Cyclohexenylmanganese Tricarbonyl. Intramolecular C–H Bond Activation via a Two-Electron, Three-Center Mn···H···C Interaction

M. Brookhart,* W. Lamanna, and M. Beth Humphrey

Contribution from the Department of Chemistry, University of North Carolina, Chapel Hill, North Carolina 27514. Received July 6, 1981

Abstract: Protonation of (η^4-cyclohexadiene)manganese tricarbonyl anion, **4**, yields neutral (η^3-cyclohexenyl)manganese tricarbonyl, **5**, in which the metal center attains an 18-electron configuration via coordination of an endo C–H bond adjacent to the π-allyl unit. The bridging hydrogen in **5** is activated and rendered acidic. Deprotonation results in regeneration of anion **4** which, upon reaction with methyl iodide, yields a mixture of the 5-*endo*-methyl and 6-*endo*-methyl derivatives of **5** (**6a** and **6b**, respectively). The Mn···H···C interaction in both **5** and **6** is best described as a closed, three-center, two-electron bond. Complex **5** undergoes three distinct fluxional isomerization processes which can be observed by variable-temperature ^{1}H and ^{13}C NMR spectroscopy: (1) exchange of the two endo C–H bonds adjacent to the allylic unit ($\Delta G^\ddagger = 8.3$ kcal/mol), (2) mutual exchange of the three carbonyl groups ($\Delta G^\ddagger = 13.1$ kcal/mol), and (3) a [1,2] metal migration about the six-membered ring ($\Delta G^\ddagger = 15.4$ kcal/mol). The first and third processes clearly result from two different modes of disruption of the three-center Mn···H···C bond in **5**. Further evidence of a three-center bonding arrangement in **5** includes an unusually small $^{13}C_1-^1H_{1-endo}$ coupling constant (85 Hz) and a thermodynamic deuterium isotope effect of 0.20 kcal/mol on the endo C–H exchange process. The existence of a strong Mn···H···C three-center interaction was confirmed by a room-temperature X-ray diffraction study of **6b** (space group $P2_1/c$, $a = 6.546$ (4) Å, $b = 9.818$ (3) Å, $c = 17.250$ (5) Å, $\beta = 112.00$ (3)°, $Z = 4$, $R_w = 0.041$). The geometry about the metal is roughly octahedral. The bridging hydrogen occupies one ligand site and is 1.86 (2) Å from manganese. The Mn–C distance is 2.301 (2) Å, and the metal-coordinated C–H bond distance is slightly elongated (1.07 (2) Å).

Current interest in aliphatic C–H bond activation by transition metals stems primarily from the need for development of homogeneous catalytic systems capable of selectively functionalizing simple aliphatic hydrocarbons.[1] Although aliphatic C–H bonds are generally inert with respect to intermolecular reactions with soluble transition-metal complexes, a few apparent examples of such reactions have been reported.[1] Intramolecular reactions of this type are much more common and typically involve insertion of an unsaturated metal center into a proximal C–H bond of one of its bound ligands. Among the most frequently encountered examples are the α-[2a,b] and β-hydride[2c] elimination reactions responsible for the decomposition of many metal–alkyl species.[3] Reactions of a transition-metal center with more remote C–H bonds are known as well;[4-7] for example, γ-CH insertion reactions leading to formation of metallacyclobutanes have recently been observed in Pt(II)[4] and Ir(I)[5] complexes. The facility of these intramolecular reactions relative to their intermolecular counterparts is often attributed to entropic effects resulting from geometrical constraints which force the C–H bond of the bound ligand into close contact with the metal atom.

Recently, it has become apparent that certain transition-metal complexes exhibit a unique mode of interaction between an unsaturated metal center and a nearby C–H bond in the ground state. In these complexes the C–H bond serves as a nonclassical donor ligand through sharing of its σ electrons with the metal and formation of a two-electron, three-center M···H···C bonding arrangement. There appears to exist an entire spectrum of three-

center interactions of this type ranging from an "open" geometry, **1**, with no carbon–metal interaction to a "closed" geometry, **2**,
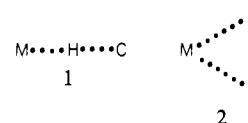
with substantial carbon–metal interaction. This type of electron-deficient, multicenter bonding is intriguing in that it serves to reduce the electron deficiency at the unsaturated metal center without cleaving the C–H bond and provides a good model for understanding the interactions which must be involved in the transition states of the intrinsically related insertion reactions described earlier.

The first clear example of a strong M···H···C interaction of this kind was observed in the pyrazolylborate complexes of molybdenum in which the three atoms assume a nearly linear or open arrangement as in **1**.[8,9] Several complexes have now been structurally characterized which exhibit closed geometries, strong metal–hydrogen interactions, and variable degrees of metal–carbon interaction.[10-14] In addition, a number of complexes have been

(1) (a) Webster, D. E. *Adv. Organomet. Chem.* **1977**, *15*, 147 and references therein. (b) Parshall, G. W. *Catalysis* **1977**, *1*, 335 and references therein.

(2) (a) Cooper, N. J.; Green, M. L. H. *J. Chem. Soc., Chem. Commun.* **1974**, 761. (b) Schrock, R. R. *J. Am. Chem. Soc.* **1975**, *97*, 6577. (c) Schrock, R. R.; Parshall, G. W. *Chem. Rev.* **1976**, *76*, 243.

(3) For a general discussion of these reactions, see: Collman, J. P.; Hegedus, L. S. "Principles and Applications of Organotransition Metal Chemistry"; University Science Books: Mill Valley, CA, 1980; p 73.

(4) Whitesides, G. M.; DiCosimo, R.; Foley, P. *J. Am. Chem. Soc.* **1980**, *102*, 6713.

(5) Tulip, T. H.; Thorn, D. L. *J. Am. Chem. Soc.* **1981**, *103*, 2448.

(6) Shaw, B. L.; Cheney, A. J.; Mann, B. F.; Slade, R. M. *J. Chem. Soc. A* **1971**, 3833.

(7) Clarke, P. W. *J. Organomet. Chem.* **1977**, *137*, 235 and references therein.

(8) (a) Trofimenko, S. *J. Am. Chem. Soc.* **1968**, *90*, 4754. (b) Trofimenko, S. *Inorg. Chem.* **1970**, *9*, 2493.

(9) (a) Cotton, F. A.; Stanislowski, A. G. *J. Am. Chem. Soc.* **1974**, *96*, 5074. (b) Cotton, F. A.; LaCour, T.; Stanislowski, A. G. *Ibid.* **1974**, *96*, 754. (c) Cotton, F. A.; Day, V. W. *J. Chem. Soc., Chem. Commun.* **1974**, 415.

(10) (a) Harlow, R. L.; McKinney, R. J.; Ittel, S. D. *J. Am. Chem. Soc.* **1979**, *101*, 7496. (b) Williams, J. M.; Brown, R. K.; Schultz, A. J.; Stucky, G. D.; Ittel, S. D. *Ibid.* **1978**, *100*, 7407. (c) Brown, R. K.; Williams, J. M.; Schultz, A. J.; Stucky, G. D.; Ittel, S. D.; Harlow, R. L. *Ibid.* **1980**, *102*, 981.

(11) (a) Beno, M. A.; Williams, J. M.; Tachikawa, M.; Muetterties, E. L. *J. Am. Chem. Soc.* **1980**, *102*, 4542. (b) Beno, M. A.; Williams, J. M.; Tachikawa, M.; Muetterties, E. L. *Ibid.* **1981**, *103*, 1485.
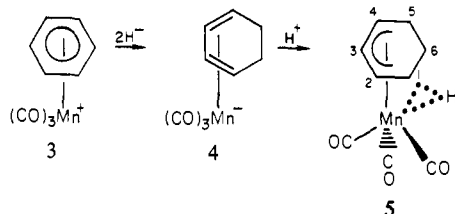
(12) (a) Schrock, R. R. *Acc. Chem. Res.* **1979**, *12*, 98 and references therein. (b) Schultz, A. J.; Williams, J. M.; Schrock, R. R.; Rupprecht, G. A.; Fellman, J. D. *J. Am. Chem. Soc.* **1979**, *101*, 1593. (c) Schultz, A. J.; Brown, R. K.; Williams, J. M.; Schrock, R. R. *Ibid.* **1981**, *103*, 169. (d) Goddard, R. J.; Hoffmann, R.; Jemmis, E. D. *Ibid.* **1980**, *102*, 7667. (e) Schrock, R. R.; Fellmann, J. D.; Messerle, L. W.; Rupprecht, G. A. *Ibid.* **1980**, *102*, 6236. (f) Schrock, R. R.; Stucky, G.; Jennische, P.; Messerle, L. W. *Ibid.* **1980**, *102*, 6744.

(13) Pasquoli, M.; Floriani, C.; Gaetani-Manfredotti, A.; Chiesi-Villa, A. *J. Am. Chem. Soc.* **1978**, *100*, 4918.

(14) Green, M.; Norman, N.; Orpen, G. *J. Am. Chem. Soc.* **1981**, *103*, 1269.

identified in which a strong M⋯H⋯C interaction is implied by spectroscopic evidence.[15-18] Although the variety of complexes is quite diverse, including both mono- and multinuclear species, all seem to share some unique properties which appear to be characteristic of these three-center, two-electron M⋯H⋯C bonding arrangements. Spectroscopically, these are manifested in terms of unusually small $^{13}C_\alpha$–$^1H_\alpha$ coupling constants and decreased C_α–H_α IR stretching frequencies, both indicative of a decrease in C–H bond order upon coordination to metal. In those cases where the M⋯H⋯C interaction has been crystallographically defined, the M–H and M–C bond distances within the three-center moiety are longer than normal M–H and M–C bond lengths. In addition, C_α–H_α bond lengths are observed to increase as a result of metal coordination and angular deformations at the α carbon are common. At least one chemical ramification of these electrophilic interactions appears to be a weakening of the coordinated C–H bond resulting in an enhanced acidity of the bridging hydrogen.[12,17]

We recently reported the synthesis of the (cyclohexadiene)-manganese tricarbonyl anion, **4**, via hydride reduction of (benz-

ene)manganese tricarbonyl cation, **3**. Protonation of the diene anion resulted in formation of cyclohexenylmanganese tricarbonyl for which the bridged structure, **5**, was proposed.[17,19] The three-center interaction in this complex renders the bridging hydrogen acidic permitting easy deprotonation and substitution of other electrophiles at carbon.[17]

In this paper we wish to report the detailed characterization of **5** and its 6-*endo*-methyl derivative based on spectroscopic and X-ray crystallographic studies. These studies allow a complete description of the structure of these complexes and provide insight into the nature of the Mn⋯H⋯C interaction and the dynamic processes which result from this interaction. The structure and dynamic properties can be compared to the related compounds, in particular, the isoelectronic [(π-enyl)iron–L_3]$^+$ complexes (L = CO, PR_3, P(OR)$_3$).

The iron tricarbonyl complexes have been spectroscopically examined by ourselves[15,20] and Olah,[21] while the phosphine and phosphite complexes have been thoroughly characterized both spectroscopically and crystallographically by groups at Du Pont and Argonne.[10,16]

Results

Synthesis of Bridged Species. Cyclohexenylmanganese tricarbonyl, **5**, was prepared by the previously reported reaction of (benzene)Mn(CO)$_3$$^+PF_6$$^-$ with two equivalents of lithium triethylborohydride followed by protonation of the resultant (1,3-cyclohexadiene)manganese tricarbonyl anion, **4**, with H$_2$O.[17] The reduction is stepwise and proceeds through a cyclohexadienyl-manganese tricarbonyl intermediate which has been identified by IR (ν_{CO} = 2010 (s), 1930 (br s) cm^{-1} in THF). Proton addition

(15) (a) Brookhart, M.; Whitesides, T. H.; Crockett, J. M. *Inorg. Chem.* **1976**, *15*, 1550. (b) Crockett, J. M. Ph.D. Dissertation, University of North Carolina, Chapel Hill, NC, 1979.

(16) Ittel, S. D.; Van-Catledge, F. A.; Tolman, C. A.; Jesson, J. P. *J. Am. Chem. Soc.* **1978**, *100*, 1317. (b) Ittel, S. D.; Van-Catledge, F. A.; Jesson, J. P. *Ibid.* **1979**, *101*, 6905.

(17) Lamanna, W.; Brookhart, M. *J. Am. Chem. Soc.* **1981**, *103*, 989.

(18) (a) Calvert, R. B.; Shapley, J. R. *J. Am. Chem. Soc.* **1977**, *99*, 5225. (b) *Ibid.* **1978**, *100*, 7726.

(19) We have learned from P. L. Pauson (private communication) that he has also obtained the bridged species **5**, by reduction of C$_6$H$_7$Mn(CO)$_3$ with lithium aluminum hydride followed by aqueous workup. See also: Pauson, P. L. *Pure Appl. Chem.* **1977**, *49*, 838; P. L. *J. Organomet. Chem.* **1980**, *200*, 207.

(20) Brookhart, M.; Harris, D. L. *Inorg. Chem.* **1974**, *13*, 1540.

(21) Olah, G. A.; Liang, G.; Yu, S. H. *J. Org. Chem.* **1976**, *41*, 2227.
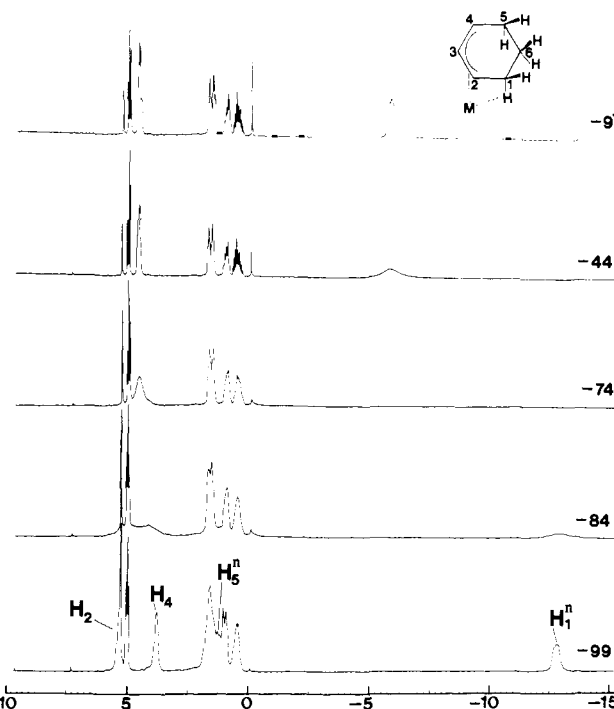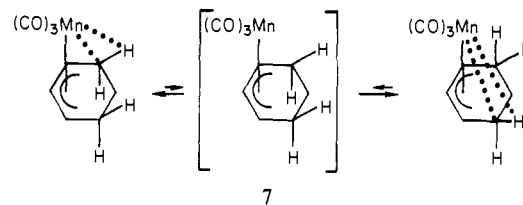
Figure 1. 100-MHz, variable-temperature ^1H NMR spectra of cyclohexenylmanganese tricarbonyl, **5**, from –99 to –9 °C in CD$_2$Cl$_2$ solvent.

Scheme I

to the diene anion is thought to be endo;[22] however, it is unclear whether the mechanism involves initial attack at the metal (i.e., formation of an intermediate diene hydride) or if the proton enters directly into the bridging position.

The bridged complex **5** is an orange liquid at room temperature (mp 0 °C) which can be distilled under vacuum and is soluble in most organic solvents. In contrast to the analogous (π-enyl)iron–L_3 cations,[15,16,21] **5** is thermally quite stable and can be heated to 120 °C without noticeable decomposition. Although **5** is slightly air sensitive, manipulation in air for short periods is possible. Elemental analysis of **5** is consistent with the proposed empirical formula (Experimental Section), and infrared spectra (pentane) exhibit three bands in the carbonyl region at 2020 (s), 1945 (s), and 1937 (s) cm^{-1} as expected for an unsymmetrical tricarbonyl complex. The ^1H and ^{13}C NMR spectra of **5** provide firm support for the assigned structure and will be discussed in detail in the following section.
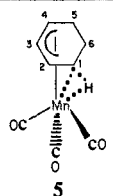
Treatment of **5** with KH results in deprotonation and regeneration of diene anion **4** which, upon reaction with excess CH$_3$I,
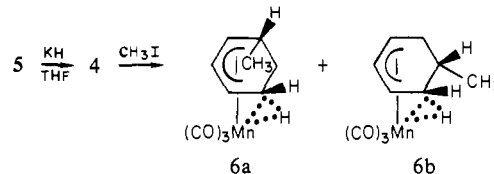
gives a 22:78 mixture of the endo-monomethylated cyclohexenyl

(22) Proton addition to the analogous neutral (diene)iron complexes proceeds exclusively endo (see ref 16). Also, reaction of the diene anion **4** with CH$_3$I results in selective transfer of the methyl group to the endo side of the ring (see this paper).

Cyclohexenylmanganese Tricarbonyl

J. Am. Chem. Soc.. Vol. 104. No. 8, 1982 2119

Table I. NMR Data for 5

structure	nu-cleus	t, °C	chem shifts (δ) and assignts^{c-e}
[structure drawing of cyclohexenyl ring labeled 1-6 with Mn(CO)₃ and H; labeled 5]	$^1H^a$	−99	H_{1-endo}, −12.8; H_{1-exo}, H_{5-exo}, 1.6; H_4 and H_2, 5.3 and 3.8; H_3, 5.0; H_{5-endo}, 1.4; H_{6-endo}, 1.0; H_{6-exo}, 0.4
	$^{13}C^b$	−100	C_1, 14.0 (dd, 146, 85 Hz); C_2 and C_4, 72.4 (d, 180 Hz) and 66.6 (d, 160 Hz); C_3, 92.9 (d, 166 Hz); C_5, 25.8 (t, 129 Hz); C_6, 15.8 (t, 133 Hz)

^{a} Recorded at 100 MHz. ^{b} Recorded at 62.9 MHz. ^{c} In CD_2Cl_2 solvent. ^{d} Shifts are in ppm relative to residual $CHDCl_2$ (^{13}C). ^{e} Undecoupled ^{13}C spectra were obtained by using gated decoupling routine. Observed coupling constants and multiplicities are shown in parentheses (d = doublet, t = triplet, q = quartet, dd = doublet of doublets).

complexes 6a and 6b, respectively. The observed isomer ratio is a result of rapid equilibration between 6a and 6b in solution as demonstrated by dynamic ^1H NMR studies.[17] Isomer 6b is conveniently isolated from this mixture as a crystalline orange solid (mp 40–42 °C) by recrystallization from petroleum ether. The structure of 6b has been determined by X-ray diffraction studies (vide infra).

Dynamic ^1H and ^{13}C NMR Studies. Complex 5 exhibits three distinct, degenerate modes of isomerization which can be observed by NMR. The isomerization with the lowest activation energy results from the degenerate equilibrium shown in Scheme I in which the two endo C–H bonds adjacent to the π-allyl unit are alternately coordinated to the metal center. This process is believed to proceed via the symmetrical 16-electron π-allyl species, 7. Whether this species represents an intermediate or a transition state in the isomerization reaction is unknown.

The series of temperature-dependent ^1H NMR spectra in CD_2Cl_2 of 5 between −9 and −99 °C (Figure 1) demonstrates the dynamic behavior resulting from this isomerization. At −99 °C exchange of the bridged and unbridged endo C–H bonds is slow on the NMR time scale, and the ^1H NMR spectrum at this temperature represents the static structure of 5. The unusually high-field resonance at −12.8 ppm is assigned to the single bridging hydrogen. The remaining assignments are summarized in Table I and are based not only on chemical shift, coupling constant, and averaging information but also on results obtained from spin saturation transfer (SST) experiments (vide infra). As the temperature is raised above −99 °C, the bridging hydrogen resonance (−12.8 ppm) and the resonance at 1.4 ppm (H_{5-endo}) broaden and eventually merge to a single two proton signal at −5.7 ppm. Similar behavior is observed for the pair of lines at 5.3 and 3.8 ppm (H_2, H_4) which average to a single resonance at 4.6 ppm. H_{1-exo} and H_{5-exo} are also expected to average as a result of the fluxional process in Scheme I; however, at −99 °C these resonances are unresolved and only minor changes in line width and peak shape are observed upon warming. Rate constants and corresponding free energies of activation for this process were estimated from the variable-temperature ^1H NMR spectra by using simple line-shape analysis,[23] the results of which are summarized in Table II.

As expected from the mechanism in Scheme I, the $^{13}C\{^1H\}$ NMR spectra of 5 are also temperature dependent. The ^{13}C NMR data for 5 at −115 °C, including shift assignments and C–H coupling constants, are summarized in Table II. Increasing the temperature above −115 °C causes the pair of lines at 72.4 and 66.6 ppm (C_2, C_4) and the pair of lines at 14.0 and 25.8 ppm (C_1, C_5) to broaden and merge. In addition, the resonances at 224.4 and 218.2 ppm, assigned to the two carbonyl carbons cis to the coordinated C–H bond, are observed to average. Figure 2 illustrates the dynamic $^{13}C\{^1H\}$ NMR behavior resulting from this low-temperature process for the pair of lines at 14.0 and 25.8 ppm.

(23) Anet, F. A. L.; Borne, A. J. R. *J. Am. Chem. Soc.* 1967, *89*, 760 and references therein.
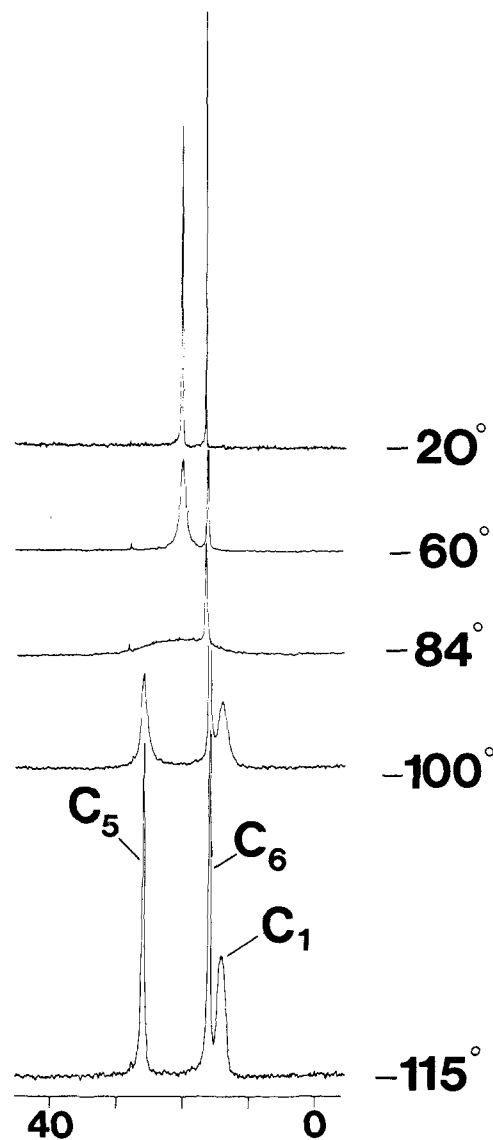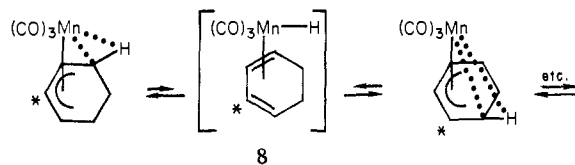

Figure 2. 62.9-MHz, variable-temperature $^{13}C\{^1H\}$ NMR spectra of cyclohexenylmanganese tricarbonyl, 5, from −115 to −20 °C in CD_2Cl_2 solvent. Only portion of the spectrum from 0 to 40 ppm is shown.

Scheme II

Again, line-shape analysis permitted calculation of rate constants and free energies of activation which compared favorably with those obtained from the ^1H NMR spectra (Table II). The average value of $\Delta G^{\ddagger}$ for all ^1H and ^{13}C measurements is 8.3 kcal/mol.

A second isomerization process is observed at much higher temperatures which is proposed to proceed through a diene hydride species, 8. In 8 the hydride can rebridge to either terminal end of the bound diene unit, permitting a degenerate [1,2] metal migration around the ring as shown by the change in the position of the label in Scheme II.

Taking into account the much more rapid endo C–H exchange process which is proceeding simultaneously, the mechanism in Scheme II predicts averaging of the three endo hydrogens and, separately, averaging of the six exo and olefinic hydrogens. As shown in the series of variable-temperature ^1H NMR spectra in toluene-d_8 between 4 and 119 °C (Figure 3), this is precisely what is observed. The spectrum at 4 °C represents the fast exchange

Table II. Summary of Rate Constants and Free Energies of Activation for Fluxional Isomerization of Cyclohexenylmanganese Tricarbonyl, 5

isomerization process	signals used	k, s^{-1}	t, °C	$\Delta G^{\ddagger}$, kcal/mol	method of calculation
endo C–H exchange	$H_{1\text{-endo}}$, $H_{5\text{-endo}}$	7.05×10^{4}	-44	8.2	^{1}H, fast exchange approx
	$H_{1\text{-endo}}$, $H_{5\text{-endo}}$	3.16×10^{3}	-68	8.6	^{1}H, coalescence approx
	H_2, H_4	3.82×10^{2}	-83	8.7	^{1}H, coalescence approx
	cis CO's	8.62×10^{2}	-89	8.1	^{13}C, coalescence approx
	C_2, C_4	8.03×10^{2}	-90	8.1	^{13}C, coalescence approx
	C_1, C_5	1.65×10^{3}	-85	8.1	^{13}C, coalescence approx
[1,2] metal migration	$H_{1\text{-endo}}$, $H_{5\text{-endo}}$	2.20×10^{2}	54	15.7	^{1}H, slow exchange approx
	$H_{1\text{-endo}}$, $H_{5\text{-endo}}$	8.41×10^{2}	69	15.5	^{1}H, slow exchange approx
	$H_A = H_{6\text{-endo}}$ $H_B = H_{1\text{-endo}}$, $H_{5\text{-endo}}$	1.26	-15	14.9	^{1}H, spin saturation transfer
	$H_A = H_{1\text{-exo}}$, $H_{5\text{-exo}}$ $H_B = H_2$, H_4	1.61	-15	14.8	^{1}H, spin saturation transfer
	C_3	1.60×10^{1}	$+20$	15.5	^{13}C, slow exchange approx
	C_2, C_4	1.92×10^{1}	$+20$	15.4	^{13}C, slow exchange approx
	C_1, C_5	1.79×10^{1}	$+20$	15.5	^{13}C, slow exchange approx
	C_6	1.76×10^{1}	$+20$	15.5	^{13}C, slow exchange approx
	C_3	9.68×10^{1}	$+40$	15.5	^{13}C, slow exchange approx
	C_2, C_4	7.98×10^{1}	$+40$	15.6	^{13}C, slow exchange approx
	C_1, C_5	8.55×10^{1}	$+40$	15.6	^{13}C, slow exchange approx
	C_6	8.36×10^{1}	$+40$	15.6	^{13}C, slow exchange approx
CO scrambling	trans CO	2.92×10^{1}	-20	13.0	^{13}C, slow exchange approx
	cis CO's	2.51×10^{1}	-20	13.1	^{13}C, slow exchange approx
	cis CO's	1.60×10^{2}	0	13.2	^{13}C, slow exchange approx

^{a} For $H_{6\text{-endo}}$, T_1 = 1.5 s, $M(0)/M(\infty)$ = 2.89. ^{b} For $H_{1\text{-exo}}$, $H_{5\text{-exo}}$, T_1 = 2.2 s, $M(0)/M(\infty)$ = 4.54.
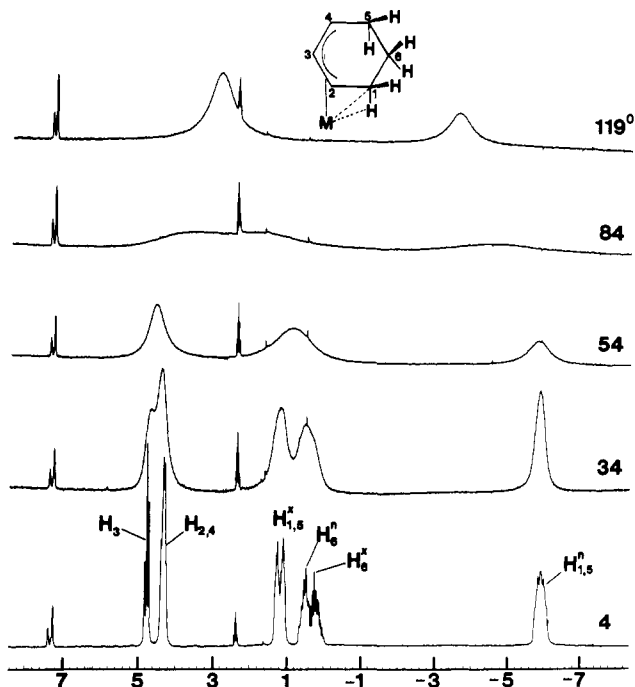

Figure 3. 100-MHz, variable-temperature ^{1}H NMR spectra of cyclohexenylmanganese tricarbonyl, 5, from 4 to 119 °C in d_8-toluene solvent.

limit for the endo C–H exchange process and the slow exchange limit for the [1,2] metal migration (chemical shifts in toluene-d_8 are somewhat different; compare Figure 1, -9 °C, with Figure 3, $+4$ °C). As the temperature is raised, the two proton resonance at -5.9 ppm ($H_{1\text{-endo}}$, $H_{5\text{-endo}}$) and the resonance at 0.5 ppm ($H_{6\text{-endo}}$) broaden and merge to a single three proton resonance at -3.7 ppm. The resonances at 4.7 (H_3), 4.3 (H_2, H_4), 1.2 ($H_{1\text{-exo}}$, $H_{5\text{-exo}}$), and 0.2 ppm ($H_{6\text{-exo}}$) average in similar fashion resulting in a single six-proton resonance at 2.8 ppm.

With regard to the ^{13}C {^{1}H} NMR spectra, the isomerization in Scheme II results in line broadening of the resonances at 15.8 (C_6), 19.9 (C_1, C_5), 69.5 (C_2, C_4), and 92.9 ppm (C_3) above room temperature. The four lines broaden at equal rates, consistent with a mechanism involving [1,2] shifts. These resonances would presumably merge to a single sharp resonance at very high temperatures; however, this was not observed due to solvent boiling

point limitations. Line shape analysis of the high temperature ^{1}H and ^{13}C{^{1}H} NMR spectra provided rate constants and free energies of activation for this second isomerization and these are again summarized in Table II.

Although the ^{1}H and ^{13}C{^{1}H} NMR line-broadening experiments provided adequate rate data for the isomerization in Scheme II, further investigations were carried out by using the Forsén and Hoffman technique of spin saturation transfer.[24] This technique, applied to the ^{1}H NMR spectrum of 5, not only provides additional rate data but also permits one to determine directly which resonances are averaging as a result of the isomerization. Such information cannot always be obtained from line-broadening experiments; for example, it is difficult to determine from the variable-temperature ^{1}H NMR spectra in Figure 3 whether the resonance at 0.2 or 0.5 ppm is averaging with the two proton resonance at -5.9 ppm ($H_{1\text{-endo}}$, $H_{5\text{-endo}}$). Spin saturation transfer experiments in this case were critical to the assignment of these resonances to $H_{6\text{-exo}}$ and $H_{6\text{-endo}}$, respectively.

Basically, the SST experiment works on the principle that the amount of saturation transferred from a saturated set of nuclei in site B to site A is proportional to the rate of site exchange and T_{1A} (the spin–lattice relaxation time of a nucleus in site A). The rate constant for exchange, k, in a two-site, equal population system is given by

$$k = \frac{1}{T_{1A}}\left[\frac{M(0)}{M(\infty)} - 1\right]$$

where $M(0)/M(\infty)$ is the ratio of the equilibrium magnetizations (integrated signal intensities) of H_A without and with saturation of H_B, respectively. The SST experiments of 5 were performed at -15 °C in CD_2Cl_2. At this temperature a significant decrease (65%) was measured in the integrated intensity of the signal at 1.0 ppm when the ($H_{1\text{-endo}}$, $H_{5\text{-endo}}$) signal (-5.7 ppm) was saturated. No other signals in the ^{1}H NMR spectrum were measurably affected. On the basis of the proposed isomerization mechanism (Scheme II), the resonance at 1.0 ppm can therefore be assigned to $H_{6\text{-endo}}$ since this is the only proton expected to exchange with $H_{1\text{-endo}}$ and $H_{5\text{-endo}}$. Similarly, saturation of (H_2, H_4) (4.6 ppm) results in a significant decrease (78%) in the area of the signal due to ($H_{1\text{-exo}}$, $H_{5\text{-exo}}$) (1.7 ppm) as well as a slight decrease (19%) in the area of the signal at 0.6 ppm. The signals due to $H_{6\text{-endo}}$ and ($H_{1\text{-endo}}$, $H_{5\text{-endo}}$) are unaffected, consistent with

(24) Forsén, S.; Hoffman, R. A. *J. Chem. Phys.* 1963, *39*, 2892.

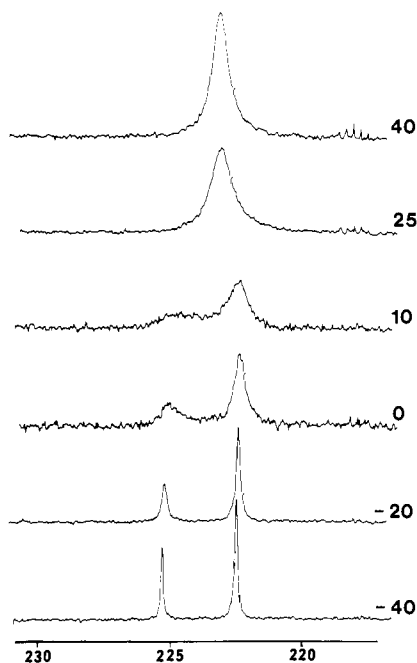*Cyclohexenylmanganese Tricarbonyl*

J. Am. Chem. Soc., Vol. 104, No. 8, 1982 2121

Figure 4. 62.9-MHz, variable-temperature ^{13}C NMR spectra of cyclohexenylmanganese tricarbonyl, 5, from -40 to 40 °C in CD_2Cl_2 solvent. Only the carbonyl region of the spectrum is shown.

Table III. Thermodynamic Parameters Derived from Deuterium Isotope Effect on Equilibrium in Equation 1

t, K	K_{eq}	ΔG, kcal/mol	ΔH, kcal/mol	ΔS, eu
317	0.74	0.19	0.22	0.07
288	0.70	0.20		
265	0.68	0.20		
255	0.67	0.20		
232	0.65	0.20		

the mechanism in Scheme II. The transfer of saturation to the resonance at 0.6 ppm upon irradiation of (H_2, H_4) permits assignment of this signal to H_{6-exo}. The reduced effect observed at this position results from the fact that transfer of saturation from (H_2, H_4) requires multiple [1,2] shifts.

Determination of T_1 values for H_{6-endo} and (H_{1-exo}, H_{5-exo}) using the fast inversion–recovery method[25] and measurement of the ratio $M(0)/M(\infty)$ for these resonances provided rate constants and the corresponding free energies of activation for the isomerization (Table II). The somewhat lower values of $\Delta G^{\ddagger}$ obtained by using this method compared to those derived from line-broadening experiments probably result primarily from errors in temperature measurement. NOE effects, which could result in the selective enhancement of certain NMR signals thereby affecting the measured relative signal intensities, may also contribute to the error in $\Delta G^{\ddagger}$. Combining the results from ^{1}H and ^{13}C NMR line-broadening experiments with the SST results permits calculation of an average value for $\Delta G^{\ddagger}$ = 15.4 kcal/mol for the [1,2] metal migration.

A third isomerization process, independent of the other two, is observed in the carbonyl region of the ^{13}C NMR spectra of 5 between -40 and +40 °C (Figure 4). As previously discussed, the low-temperature endo C–H exchange process averages two of the carbonyl resonances resulting in the 2:1 pattern of lines at 221.7 (CO's cis to H_{1-endo}) and 226.2 ppm (CO trans to H_{1-endo}). Above -40 °C the cis carbonyl groups begin to rapidly exchange with the single trans carbonyl causing these lines to broaden and merge to a single resonance at 223.9 ppm. Since the trans CO can exchange with only one of the two cis CO's, the downfield signal broadens twice as fast as the upfield signal. The temperature-dependent spectra provide no detailed information relating to the mechanism of this mutual exchange process; however, some likely mechanistic schemes will be discussed in the following section. Rate constants and free energies of activation calculated by line shape analysis are given in Table II ($\Delta G^{\ddagger}_{av}$ = 13.1 kcal/mol).

Deuterium-Labeling and Thermodynamic Isotope Effect. The reaction of (cyclohexadienyl-d_7)manganese tricarbonyl with lithium triethylborohydride and quenching of the intermediate diene anion with D_2O proceeds quantitatively and results in a mixture of isotopically labeled derivatives of 5. The ^{1}H NMR

spectrum of the isolated product indicates ^{1}H incorporation into both the exo and endo positions; however, the extent of ^{1}H incorporation into each position could not be ascertained. The presence of at least two endo ^{1}H in a major fraction of the product suggests that endo ^{1}H/^{2}H exchange during the workup is at least partially responsible for the resultant mixture.[26] It is possible that some of the endo ^{1}H results from endo attack of hydride on the cyclohexadienyl ring,[27] although, in general, attack of nucleophiles on polyolefin ligands is exclusively exo.

The presence of both ^{1}H and ^{2}H in the endo positions of this material results in some unusual ^{1}H NMR features. At 15 °C two resonances are observed upfield of Me_4Si. The major resonance (-5.8 ppm) is unshifted with respect to the resonance observed in the unlabeled complex, 5, and results from rapid endo C–H exchange in the "symmetrically labeled" species containing only ^{1}H in the 1-endo and 5-endo position. The minor resonance is shifted 1.2 ppm upfield (-7.0 ppm) and arises from the equilibrium shown in eq 1 in which either ^{1}H or ^{2}H can occupy the

(1)
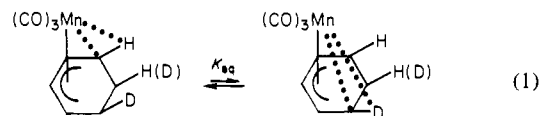
bridge position. The chemical shift of the minor resonance is determined by the weighted average of the terminal and bridging ^{1}H shifts and is therefore a function of K_{eq}. The upfield shift of this signal relative to the major resonance indicates that ^{1}H competes more effectively than ^{2}H for the bridge site and represents a substantial isotope effect on the equilibrium constant. The predominance of the ^{1}H-bridged form is understandable in terms of the relative differences in the zero-point energies of the terminal and bridging C–H and C–D bonds. This difference is expected to be greatest when C–H and C–D are terminal. Coordination to metal results in substantial weakening of these bonds (as indicated by the small C_1–H_{1-endo} coupling constant in 5 of 85 Hz, Table I) and a decrease in their relative zero-point energy gap. Since the zero-point energy of a C–D bond is lower than a C–H bond (terminal or bridging), C–D in the "unsymmetrically labeled" complex prefers to remain terminal, shifting the equilibrium in eq 1 in favor of the ^{1}H-bridged form. Similar effects have been observed in partially deuterated (η^3-butenyl)- and (η^3-cyclooctenyl)iron tris(phosphite) complexes[16b] as well as in Shapley's methyl-bridged osmium cluster.[18b]

The chemical shift of the minor resonance is temperature dependent and varies from -7.3 ppm at -41 °C to -6.9 ppm at 44 °C. The equilibrium constant, K_{eq}, was calculated from the chemical shift data at various temperatures within this range (Table III). From the relationship $\Delta G = -RT \ln K_{eq}$ the free energy difference between the ^{1}H-bridged and ^{2}H-bridged forms was determined (Table III), giving an average value of 0.20 kcal/mol. This can be compared to a smaller of 0.13 kcal/mol for the thermodynamic isotope effect in the methyl-bridged cluster $Os_3(CO)_{10}CH_2D_2$,[18b] suggesting a stronger M···H···C interaction in the manganese system. A least squares plot of $\ln K_{eq}$ vs. $1/T$ over the entire temperature range gave a straight line with a correlation coefficient of 0.984. The slope and y intercept provided values for ΔH = 0.22 kcal/mol and ΔS = 0.07 eu, respectively. The negligible value for ΔS is not surprising since the isotopic

(25) Canet, D.; Levy, G. C. *J. Magn. Reson.* **1975**, *18*, 199.

(26) Solutions of 5 in CH_3OD undergo endo ^{1}H/^{2}H exchange over a period of days.
(27) Faller, J. W. *Inorg. Chem.* **1980**, *19*, 2857.

2122 *J. Am. Chem. Soc., Vol. 104, No. 8, 1982*

Brookhart, Lamanna, and Humphrey

Table IV. Final Positional[a] and Thermal Parameters[b] $(U_{ij} \times 10^2)$ for $[(\eta^3\text{-}C_6H_8(CH_3))]Mn(CO)_3$, 6b

atom	x	y	z	U_{11}	U_{22}	U_{33}	U_{12}	U_{13}	U_{23}
Mn	0.36800 (8)	0.23253 (5)	0.05789 (3)	4.14 (2)	3.95 (2)	4.05 (2)	0.58 (3)	0.73 (3)	−0.12 (3)
O(1)	0.3705 (5)	0.1694 (4)	−0.1089 (2)	9.9 (2)	12.6 (2)	5.4 (1)	−2.2 (2)	2.6 (1)	1.7 (2)
O(2)	−0.0691 (4)	0.3468 (3)	−0.0316 (2)	5.4 (1)	7.4 (2)	7.2 (2)	2.0 (1)	0.4 (1)	0.9 (2)
O(3)	0.1676 (5)	−0.0157 (3)	0.0952 (2)	8.3 (2)	5.9 (2)	10.2 (2)	−1.5 (2)	1.3 (2)	1.6 (2)
C(1)	0.7432 (5)	0.2421 (4)	0.1296 (2)	4.2 (1)	5.2 (2)	5.2 (2)	−0.0 (2)	1.5 (1)	0.3 (2)
C(2)	0.6221 (6)	0.3704 (4)	0.0962 (2)	5.1 (2)	4.7 (2)	5.4 (2)	−0.5 (2)	0.7 (2)	1.1 (2)
C(3)	0.4725 (6)	0.4069 (3)	0.1319 (2)	6.2 (2)	3.6 (2)	5.4 (2)	0.6 (2)	−0.1 (2)	−0.7 (2)
C(4)	0.4260 (5)	0.3094 (4)	0.1822 (2)	4.9 (2)	6.1 (2)	4.8 (2)	1.0 (2)	1.9 (1)	−0.9 (2)
C(5)	0.6087 (6)	0.2265 (4)	0.2448 (2)	6.3 (2)	6.0 (2)	3.9 (2)	0.7 (2)	1.3 (1)	−0.1 (2)
C(6)	0.8154 (5)	0.2264 (4)	0.2244 (2)	4.8 (2)	4.3 (2)	4.9 (2)	−0.2 (2)	0.4 (1)	0.1 (2)
C(7)	0.9553 (6)	0.1003 (4)	0.2565 (2)	6.1 (2)	6.2 (2)	6.7 (2)	1.4 (2)	0.8 (2)	1.0 (2)
C(8)	0.3755 (6)	0.1923 (4)	−0.0431 (2)	5.0 (2)	6.4 (2)	5.9 (2)	1.2 (2)	1.1 (2)	−0.1 (2)
C(9)	0.1029 (5)	0.3033 (3)	0.0042 (2)	5.1 (2)	4.5 (2)	4.8 (2)	0.1 (2)	1.5 (1)	−0.2 (2)
C(10)	0.2439 (6)	0.0788 (4)	0.0790 (2)	5.0 (2)	5.3 (2)	5.7 (2)	0.8 (2)	0.1 (2)	−0.1 (2)

atom	x	y	z	B, Å^2	atom	x	y	z	B, Å^2
H(1A)	0.645 (4)	0.153 (3)	0.106 (2)	3.8 (7)	H(5B)	0.633 (4)	0.260 (3)	0.300 (2)	4.7 (8)
H(1B)	0.862 (4)	0.224 (3)	0.105 (2)	4.2 (7)	H(6)	0.905 (4)	0.310 (3)	0.248 (2)	4.3 (7)
H(2)	0.659 (5)	0.423 (3)	0.058 (2)	4.9 (8)	H(7A)	0.094 (5)	0.104 (3)	0.246 (2)	5.8 (9)
H(3)	0.386 (4)	0.488 (3)	0.114 (2)	3.9 (7)	H(7B)	0.887 (4)	0.021 (3)	0.233 (2)	4.3 (7)
H(4)	0.308 (4)	0.321 (3)	0.198 (2)	3.6 (7)	H(7C)	0.090 (4)	0.085 (3)	0.314 (2)	5.0 (8)
H(5A)	0.552 (4)	0.128 (3)	0.245 (2)	4.2 (7)					

[a] x, y, and z are fractional coordinates. Estimated standard deviations in parentheses. [b] The form of the anisotropic temperature factor is $\exp[-2\pi^2(U_{11}h^2a^{*2} + U_{22}k^2b^{*2} + U_{33}l^2c^{*2} + 2U_{12}hka^*b^* + 2U_{13}hla^*c^* + 2U_{23}klb^*c^*)]$.

site preferences in the labeled complex are expected to be determined almost exclusively by ΔH.

X-ray Crystal Structure of (6-endo-Methylcyclohexenyl)manganese Tricarbonyl, 6b. Although 5 is a crystalline solid at low temperatures, its low melting point (0 °C) precluded a room temperature X-ray structure determination. The methyl derivative 6, however, is a solid at room temperature, and crystals suitable for X-ray analysis were easily obtained. Although ^{1}H NMR studies indicate the presence of two isomers, 6a and 6b, in solution, the crystal examined consisted of a single isomer, 6b.

The 6-endo-methyl in 6b is expected to have no effect on the structural features of the Mn···H···C interaction. This contention is supported by spectroscopic evidence; for example, the ^{1}H chemical shift of the bridging hydrogen in 6b (−13.1 ppm at −110 °C) is nearly identical with that observed in 5 (−12.8 ppm at −100 °C). Therefore, the structural details determined for 6b should be generally applicable to the parent complex 5.

The structure of 6b is shown in Figure 5, and the final positional and thermal parameters are given in Table IV. Table V lists the bond distances and pertinent bond angles.

The geometry about the manganese atom is roughly octahedral. The bridging hydrogen occupies the ligand site approximately trans to one carbonyl ligand [H(1A)–Mn–C(9) = 175.2 (6)°] and cis to two carbonyls [H(1A)–Mn–C(8) = 87.9 (6)° and H(1A)–Mn–C(10) = 89.9 (7)°]. The two remaining ligand sites are occupied by the allylic portion of the cyclohexenyl ring which adopts an eclipsed conformation with respect to the carbonyl ligands, as expected for a nominally 16-electron complex.[28]

The Mn–H(1A) distance of 1.86 (2) Å and the Mn–C(1) distance of 2.301 (2) Å confirm the existence of a strong Mn··H··C interaction in 6b. These distances, as well as the Mn–H–(1A)–C(1) angle of 100 (1)°, are comparable to those found in the neutron diffraction study of the similarly bridged $[(\eta^3\text{-}C_8H_{13})Fe(P(OCH_3)_3)_3^+][BF_4]^-$ complex, 9 (1.874 (3) Å, 2.362 (2) Å, and 99.4 (2)°, respectively).[10c] Also noteworthy is the apparent elongation of the C(1)–H(1A) bond distance to 1.07 (2) Å as a result of metal coordination of the C–H bonding electrons. The other C–H bond distances in the molecule are shorter and range from 0.92 (2) to 1.04 (2) Å. C–H bond lengths are systematically underestimated by X-ray diffraction, and actual distances will be greater (see below).

The Mn–C(8) and Mn–C(10) distances for the carbonyl ligands cis to the bridging hydrogen are 1.805 (3) Å and 1.814 (3) Å,
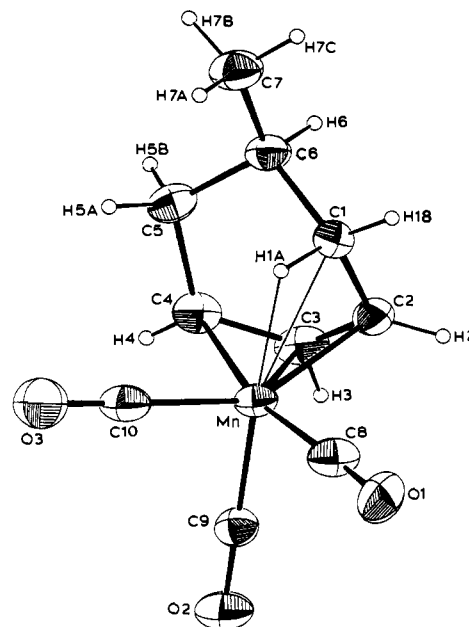

Figure 5. Molecular structure of $[\eta^3\text{-}C_6H_8(CH_3)]Mn(CO)_3$, 6b. Non-hydrogen atoms are represented by their 30% probability ellipsoids for thermal motion. Hydrogen atoms are represented by spheres of arbitrary size.

respectively. The Mn–C(9) bond length of 1.775 (3) Å for the trans carbonyl is significantly shorter. Similar contractions of the M–C bond trans to a hydride ligand have been noted in HMn(CO)$_5$ (Mn–C$_{cis}$(av) = 1.853 (13) Å; Mn–C$_{trans}$ = 1.822 (12) Å)[29] as well as in other metal carbonyl hydrides.[30]

The Mn···H(1A)···C(1) interaction results in some distortion of the cyclohexenyl ligand. The allylic portion of the ring is unsymmetrically bound to manganese; the Mn–C(2) distance is shortest at 2.053 (3) Å, the Mn–C(3) distance is 2.092 (2) Å, and the Mn–C(4) distance is longest at 2.168 (3) Å. This differs from the geometry seen in many metal allyl complexes in which the allyl ligand is symmetrically bound to the metal with the

(28) Albright, T. A.; Hofmann, P.; Hoffmann, R. *J. Am. Chem. Soc.* **1977**, *99*, 7546.

(29) LaPlaca, S. J.; Hamilton, W. C.; Ibers, J. A.; Davison, A. *Inorg. Chem.* **1969**, *8*, 1928.

(30) Frenz, B. A.; Ibers, J. A. In "Transition Metal Hydrides"; Muetterties, E. L., Ed.; Marcel Dekker: New York, 1971; pp 41–3.

Table V. Selected Bond Distances (Å) and Angles (Deg) for
$[\eta^3\text{-}C_6H_8(CH_3)]Mn(CO)_3$, 6b

Distances			
Mn–C(1)	2.301 (2)	Mn–H(1A)	1.86 (2)
Mn–C(2)	2.053 (3)	Mn–C(8)	1.805 (3)
Mn–C(3)	2.092 (2)	Mn–C(9)	1.775 (3)
Mn–C(4)	2.168 (3)	Mn–C(10)	1.814 (3)
C(1)–C(2)	1.485 (3)	C(4)–H(4)	0.92 (2)
C(1)–C(6)	1.530 (2)	C(5)–C(6)	1.520 (4)
C(1)–H(1A)	1.07 (2)	C(5)–H(5A)	1.04 (2)
C(1)–H(1B)	1.03 (2)	C(5)–H(5B)	0.96 (2)
C(2)–C(3)	1.385 (4)	C(6)–C(7)	1.516 (4)
C(2)–H(2)	0.94 (2)	C(6)–H(6)	1.00 (2)
C(3)–C(4)	1.400 (4)	C(7)–H(7A)	0.99 (2)
C(3)–H(3)	0.96 (2)	C(7)–H(7B)	0.92 (2)
C(4)–C(5)	1.514 (3)	C(7)–H(7C)	0.95 (2)
C(8)–O(1)	1.146 (3)	C(10)–O(3)	1.137 (3)
C(9)–O(2)	1.145 (3)		

Angles Involving the Mn Atom			
C(1)–Mn–C(2)	39.4 (1)	C(2)–Mn–C(10)	148.6 (1)
C(1)–Mn–C(3)	39.0 (1)	C(3)–Mn–C(4)	38.3 (1)
C(1)–Mn–C(4)	72.4 (1)	C(3)–Mn–C(8)	130.3 (1)
C(1)–Mn–C(8)	96.8 (1)	C(3)–Mn–C(9)	91.8 (1)
C(1)–Mn–C(9)	154.5 (1)	C(3)–Mn–C(10)	128.8 (1)
C(1)–Mn–C(10)	113.2 (1)	C(4)–Mn–C(8)	166.6 (1)
C(1)–Mn–H(1A)	27.4 (7)	C(4)–Mn–C(9)	98.9 (1)
H(1A)–Mn–C(2)	66.2 (7)	C(4)–Mn–C(10)	90.9 (1)
H(1A)–Mn–C(3)	91.9 (7)	C(8)–Mn–C(9)	87.5 (1)
H(1A)–Mn–C(4)	85.9 (6)	C(8)–Mn–C(10)	100.8 (1)
H(1A)–Mn–C(8)	87.7 (6)	C(9)–Mn–C(10)	90.4 (1)
H(1A)–Mn–C(9)	175.2 (6)	Mn–H(1A)–C(1)	100 (1)
H(1A)–Mn–C(10)	89.9 (7)	Mn–C(3)–C(2)	69.0 (1)
C(2)–Mn–C(3)	39.0 (1)	Mn–C(4)–C(3)	38.3 (1)
C(2)–Mn–C(4)	68.4 (1)	Mn–C(8)–O(1)	176.7 (2)
C(2)–Mn–C(8)	98.2 (1)	Mn–C(9)–O(2)	178.6 (2)
C(2)–Mn–C(9)	115.2 (1)	Mn–C(10)–O(3)	177.5 (3)

Angles within the Cyclohexenyl Ring			
C(2)–C(1)–C(6)	113.9 (2)	C(4)–C(5)–C(6)	111.6 (2)
C(6)–C(1)–H(1A)	103 (1)	C(4)–C(5)–H(5A)	108 (1)
C(6)–C(1)–H(1B)	116 (1)	C(4)–C(5)–H(5B)	109 (1)
C(2)–C(1)–H(1A)	113 (1)	C(6)–C(5)–H(5A)	110 (1)
C(2)–C(1)–H(1B)	111 (1)	C(6)–C(5)–H(5B)	113 (1)
H(1A)–C(1)–H(1B)	98 (1)	H(5A)–C(5)–H(5B)	104 (2)
C(1)–C(2)–C(3)	114.3 (2)	C(5)–C(6)–C(1)	107.6 (2)
C(1)–C(2)–H(2)	120 (1)	C(5)–C(6)–C(7)	112.6 (2)
C(3)–C(2)–H(2)	126 (1)	C(8)–C(6)–C(1)	112.0 (2)
C(2)–C(3)–C(4)	116.9 (2)	C(5)–C(6)–H(6)	110 (1)
C(2)–C(3)–H(3)	120 (1)	C(1)–C(6)–H(6)	108 (1)
C(4)–C(3)–H(3)	122 (1)	C(7)–C(6)–H(6)	110 (1)
C(3)–C(4)–C(5)	120.9 (2)	C(6)–C(7)–H(7A)	112 (2)
C(3)–C(4)–H(4)	120 (1)	C(6)–C(7)–H(7B)	114 (2)
C(5)–C(4)–H(4)	112 (1)	C(6)–C(7)–H(7C)	112 (2)

shortest M–C bond being to the central carbon.[31] In (η^3-C_3H_5)Mn(CO)$_2$[P(OCH$_3$)$_3$]$_2$,[32] for instance, the Mn–C(1) distance is 2.223 (17) Å, the Mn–C(2) separation is 2.114 (15) Å, and the Mn–C(3) distance is 2.229 (13) Å. In 6b, however, the Mn–H(1A)–C(1) interaction displaces C(2) toward the metal and tilts the allyl portion of the ring so that the dihedral angle between the allylic plane (C(2),C(3),C(4)) and the axial plane (Mn,C-(9),H(1A)) is 115.2°. The dihedral angle between the allylic plane and the equatorial plane (Mn,C(8),C(10)) is 126.8°; the corresponding angle in 9 is 131.57 (5)°.[10c]

In general, the distortions of the bond distances and angles in the cyclohexenyl ring are less pronounced than those observed for the eight-membered ring in 9. The C(6)–C(1) distance in 6b of 1.530 (3) Å is comparable to the C(6)–C(5) separation of 1.520 (4) Å, and the C(1)–C(2)–C(3) angle of 114.3 (2)° approaches the C(3)–C(4)–C(5) angle of 120.9 (2)°. In 9, however, the C(1)–C(2)–C(3) angle (118.6 (1)°) differs significantly from the C(3)–C(4)–C(5) angle (127.3 (1)°).[10c]

(31) Clarke, H. L. *J. Organomet. Chem.* **1974**, *80*, 155.
(32) Brisdon, B. J.; Edwards, D. A.; White, J. W.; Drew, M. G. B. *J. Chem. Soc., Dalton Trans.* **1980**, 2129.

The methyl group of the cyclohexenyl ring is located at the 6-endo position, and the C(6)–C(7) bond length is a normal 1.516 (4) Å.

In the allylic portion of the ring the C(2)–C(3) and C(3)–C(4) bond lengths of 1.385 (4) and 1.400 (4) Å are predictably shorter than the aliphatic C–C bonds in the ring which range from 1.530 (2) to 1.514 (3) Å. It is noteworthy that the C(1)–C(2) bond length (1.485 (3) Å) is significantly shorter than the corresponding C(4)–C(5) distance (1.514 (3) Å) on the opposite side of the ring, suggesting partial multiple bond character in the C(1)–C(2) bond. A similar feature was noted in the structure of 9, in which C-(1)–C(2) = 1.500 (2) Å and C(4)–C(5) = 1.532 (2) Å.[10c]

Discussion

Several examples of cationic (π-enyl)iron–L$_3$ complexes of general structure 10 which exhibit a three-center Fe···H···C in-

10
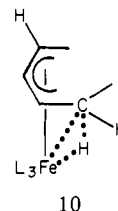
teraction have now been reported.[10,15a,16] These species have all been generated from the corresponding neutral (diene)iron–L$_3$ complexes via protonation in acids with noncoordinating anions. Although earlier studies of the protonation of (diene)iron complexes had been performed,[33] the first suggestion that these protonated species may possess a hydrogen-bridged structure was made by Brookhart and Whitesides[15a] on the basis of the unusual value of $J_{^{13}C_1-^1H_{1-endo}}$ (78–88 Hz) in protonated (cyclohexadiene)iron tricarbonyl. This value was too low to attribute to a full C–H bond but too high for a species containing a terminal iron–hydride bond and no direct hydrogen–carbon bonding. Ittel has carried out an extensive study of the structure and dynamics of a series of protonated (diene)iron–L$_3$ species where L = phosphite or phosphine.[10,16] The structural characterization of the bridging interaction culminated in a neutron diffraction study of (η^3-C_8H_{13})Fe[P(OCH$_3$)$_3$]$_3^+$, 9, by the Du Pont and Argonne groups in which the bridging hydrogen was precisely located.[10c] The bridged manganese species, 5 and 6, are isoelectronic with the cationic (π-enyl)iron systems and several structural and dynamic features of the manganese system parallel those of the iron system. These features will be compared and contrasted throughout this discussion.

Structural Features. The nature of the bridging interaction is of central importance to understanding the structures and dynamics of 5 and 6. We believe that the Mn···H(1A)···C(1) interaction can best be described as a "closed" two-electron, three-center bond in which a substantial bonding interaction exists between Mn and both C(1) and H(1A). The triangular arrangement of these atoms is clear. The Mn–H(1A)–C(1) angle in 6b is 100 (1)° and is comparable to the corresponding angle of 99.42 (2)° in the iron complex 9. Both the Mn–C(1) distance of 2.301 (2) Å and the Mn–H(1A) separation of 1.86 (2) Å are ca. 0.15 Å longer than the sums of the appropriate covalent radii (Mn = 1.39, C = 0.77, and H = 0.37 Å);[34] however, the distances are sufficiently short to indicate substantial Mn–C(1) and Mn–H(1A) bonding interactions. Mn–C bond lengths approaching 2.30 Å are known. For example, long Mn–C distances to the terminal carbons of π-dienyl ligands are not unusual; in (azulene)dimanganese hexacarbonyl the average terminal Mn–C distance is 2.279 (10) Å.[35] In cyclohexadienylmanganese tricarbonyl the corresponding Mn–C distance is 2.19 (7) Å[36] and

(33) A review of the early work in this area is contained in reference 15a.
(34) Huheey, J. E. "Inorganic Chemistry—Principles of Structure and Reactivity"; Harper and Row: New York, 1972; p 232.
(35) Churchill, M. R.; Bird, P. H. *Inorg. Chem.* **1968**, *7*, 1793.
(36) Churchill, M. R.; Scholer, F. R. *Inorg. Chem.* **1969**, *8*, 1950.

Table VI. $^{13}C^{-1}H$ Coupling Constants for C-H Bonds Coordinated to Metal

complex	$J^{13}C^{-1}H$, Hz	ref
$[(\eta^3\text{-butenyl})Fe(CO)_3][BF_4]$	74	15b, 21
$[(\eta^3\text{-butenyl})Fe(CO)_2(P(OMe)_3)][BPh_4]$	84	16b
$[(\eta^3\text{-butenyl})Fe(P(OMe)_3)_3][BPh_4]$	~100	16b
$[(\eta^3\text{-cycloheptenyl})Fe(P(OMe)_3)_3][BPh_4]$	80	16b
$[(\eta^3\text{-cyclohexenyl})Fe(CO)_3][SO_3F]$	78–88	15
$[(\eta^3\text{-cyclohexenyl})Fe(CO)_2(P(OMe)_3)][SO_3F]$	81	15b
$[Ta(CHCMe_3)Cl_3(PMe_3)]_2$	101	12a
$Ta(\eta^5\text{-}C_5Me_5)(CHCMe_3)(\eta^2\text{-}C_2H_4)(PMe_3)$	74	12c
$(\eta^3\text{-cyclohexenyl})Mn(CO)_3$	85	this work

Table VII. Free Energies of Activation for Endo C-H Exchange and Methyl Group Rotation

complex	$\Delta G^{\ddagger}$, kcal/mol	ref
$[(\eta^3\text{-cyclooctenyl})Fe(P(OMe)_3)_3][BPh_4]$	<5	16b
$[(\eta^3\text{-cycloheptenyl})Fe(P(OMe)_3)_3][BPh_4]$	10.4	16b
$[(\eta^3\text{-cyclohexenyl})Fe(P(OMe)_3)_3][BPh_4]$	10.0	16b
$[(\eta^3\text{-cyclohexenyl})Fe(CO)_3][BF_4]$	10.6	15
$(\eta^3\text{-cyclohexenyl})Mn(CO)_3$	8.3	this work
$[(\eta^3\text{-butenyl})Fe(CO)_3][BF_4]$	10.2	15b
$[(\eta^3\text{-butenyl})Fe(P(OMe)_3)_3][BPh_4]$	8.8	16b
$[(\eta^3\text{-butenyl})Fe(PMe_3)_3][BPh_4]$	8.5	16b

in $[\eta^5\text{-}C_5H_5(C_9H_5O_2)Mn(CO)_3]^{37}$ Mn–C bond lengths of 2.21 (2) Å were reported. Interestingly, the Mn–C(1) distance in **6b** is slightly shorter than the Fe–C(1) separation, 2.363 (2) Å,[10c] in **9**, despite the smaller covalent radius of iron (Fe = 1.25 Å).[34]

Although the Mn–H(1A) distance in **6b** is longer than typical values for Mn–H bonds in terminal metal hydrides such as $HMn(CO)_5$ (Mn–H = 1.601 (16) Å), it is within the range of Mn–H bonds to bridging hydrogens. In $H_3Mn_3(CO)_{12}$[38] the average Mn–H bond distance is 1.72 (3) Å and in $HMn_2(C-O)_8[P(C_6H_5)_3]_2$[39] the Mn–H separation is 1.86 (6) Å. In addition, the fact that H(1A) clearly occupies an octahedral ligand site in **6b** indicates a strong Mn–H(1A) interaction.[40]

An interesting consequence of the three-center interaction is the apparent elongation of the C(1)–H(1A) bond. The observed distance of 1.07 (2) Å is greater than any other C–H bond in **6b**. Due to the systematic underestimation of C–H bond distances by X-ray diffraction,[9b] this probably represents a lower limit for the actual C–H distance and may indicate an actual C–H bond distance approaching 1.17 Å. Substantial errors arise in determining C–H distances, and therefore these values must be interpreted with caution. More accurate comparisons must await a neutron diffraction study. The C(1)–H(1A) bond distance determined by neutron diffraction in the analogous cyclooctenyliron complex, **9**, is 1.164 (3) Å. In both the iron and manganese systems the C(1)–H(1A) elongation implies a weakening of the C–H bond due to a decrease in C–H bond order upon coordination to metal. This is strongly supported by both deuterium isotope effects and $J^{13}C^{-1}H$ data. Weakening of the C–H bond results in a smaller zero-point energy difference between Mn···H···C and Mn···D···C as compared to "terminal" C–H vs. C–D. Thus, as described above, in partially deuterated samples of **5** where ^1H and ^2H compete for terminal and bridging sites, ^2H prefers to occupy a terminal, unbridged site. The reduced C_1–$H_{1\text{-endo}}$ bond order in **5** also gives rise to an unusually small $^{13}C_1$–$^1H_{1\text{-endo}}$ coupling constant of 85 Hz. Decreased coupling constants are typical of C–H bonds coordinated to transition metals, and for comparison Table VI summarizes $J^{13}C^{-1}H$ values for a variety of such complexes. An obvious trend, for structurally similar compounds, is that $J^{13}C^{-1}H$ decreases as the metal becomes more electrophilic, indicating an increase in the degree of interaction between the metal and the C–H bond.

One additional structural feature which should be noted is the C(1)–C(2) bond length of 1.485 (3) Å in **6b**. This is significantly shorter than the distance expected for a C–C single bond (1.54 Å)[41] and suggests partial double-bond character in the C(1)–C(2) bond indicative of the carbon skeleton in the bridged structure being intermediate between the π-allyl formulation **7** and the diene structure **8**. Consistent with the decreased C(1)–C(2) distance in **6b** is the value of $J^{13}C^{-1}H_{H1\text{-exo}}$ (146 Hz, see Table I) for **5**. This is significantly higher than the other aliphatic C–H couplings in **5** and is likely a result of partial sp² rehybridization of C(1) upon interaction with the metal center.

Dynamic Processes. Two of the dynamic processes exhibited by **5** are clearly related to the different modes of disruption of the two-electron, three-center bond. From the bridged structure, **5**, the unsaturated species **7** is accessible through "dechelation"

7   5   8
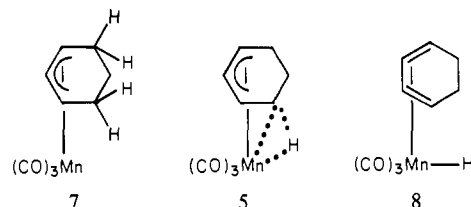
of the C–H bond from manganese while cleavage of the C–H bond results in formation of the manganese diene hydride **8**. Interestingly, the manganese complex, unlike the analogous iron systems, is sufficiently thermally stable that *both* of these processes can be studied by dynamic ^1H and ^{13}C NMR spectroscopy as described in the results section.

The low-temperature dynamic process with $\Delta G^* = 8.3$ kcal/mol clearly represents exchange of the two endo C–H bonds adjacent to the allylic unit between bridging and "terminal" sites via unsaturated **7**. Similar endo C–H bond exchange has been observed in a number of cyclic (π-enyl)iron-L_3^+ complexes with ring sizes ranging from 6 to 8.[16b] The rate of exchange in these complexes was found to be a function of ring size and the relative donor and acceptor properties of the ligands L. For the acyclic (η^3-butenyl)iron-L_3^+ complexes, dechelation of the C–H bond and formation of a 16-electron π-allyl species permit free rotation of the terminal methyl group. The rate of methyl rotation in these systems is also dependent on the electronic properties of the ancillary ligands. Free energies of activation for endo C–H exchange and methyl rotation in a few chosen examples are summarized in Table VII. Examination of this table indicates that replacing carbonyl ligands with better donor ligands such as phosphines or phosphites increases the rate of exchange. This may be rationalized in terms of better donor ligands stabilizing the electron-deficient π-allyl species relative to the 18-electron hydrogen-bridged ground state. The manganese complex **5** fits this trend in that *neutral* **5** undergoes more rapid endo C–H bond exchange than the analogous cationic complex, $(\eta^3\text{-}C_6H_9)Fe(CO)_3^+$ ($\Delta G^* = 11$ kcal/mol).[15] The cationic 16-electron (π-allyl)iron species analogous to **7** is expected to be more electrophilic than **7**.

(37) Barrow, M. J.; Mills, O. S. *Acta Crystallogr., Sect. B* **1974**, *B30*, 1635.

(38) Kirtley, S. W.; Olsen, J. P.; Bau, R. *J. Am. Chem. Soc.* **1973**, *95*, 4532.

(39) Doedens, R. J.; Robinson, W. T.; Ibers, J. A. *J. Am. Chem. Soc.* **1967**, *89*, 4323.

(40) A reviewer has suggested that it may be incorrect to term the Mn–C–H interaction "chelating" or alternatively the three-center interaction as "closed". The objections to this formulation center on the fact that the hydrogen atom is located at the octahedral site and that the close approach of C(1) to Mn may therefore "be simply due to geometrical constraints of the molecule". Similar arguments have been applied to the bridged iron complex **9**.[10c] We believe that regardless of whether C(1) is "forced" into close proximity to the metal by the Mn–H(1A) interaction or not, the fact that the Mn–C(1) distance of 2.301 (2) Å is within bonding range indicates that this system is most simply and aptly described as a "closed" interaction.

(41) Sutton, L. E. "Tables of Interatomic Distances and Configuration in Molecules and Ions". Supplement 1956–1959 The Chemical Society: London, 1965; p S14s.

The high-temperature dynamic process observed for **5** with $\Delta G^{\ddagger}$ = 15.4 kcal/mol must involve formation of diene hydride **8** and, as described earlier, results in a [1,2] manganese migration about the ring. A detailed comparison with the iron systems cannot be made since no rates or activation energies are available for these cases.

Evidence for a [1,2] metal migration in the iron system is limited to the results obtained from deuteration studies. Reaction of cyclic or acyclic (diene)iron tris(phosphite) complexes with D^{+} results in statistical incorporation of a single deuterium into all endo positions (or terminal positions in the acyclic case) of the resulting bridged π-enyl species.[16b] The deuterium scrambling between these positions is obviously a result of isomerization through a diene hydride intermediate. The lack of dynamic NMR evidence for this isomerization stems from the relatively low thermal stability of the cationic iron complexes.

The third dynamic process we must consider is that which results in mutual exchange of all three carbonyl ligands in **5**, $\Delta G^{\ddagger}$ = 13.1 kcal/mol. Similar exchange of the three phosphorous ligands in $(\eta^{3}\text{-}C_{6}H_{9})Fe[P(OCH_{3})_{3}]_{3}^{+}$ has been observed by $^{31}P\{^{1}\}$ NMR spectroscopy.[16b] The activation barrier (15.9 kcal/mol) for phosphorous scrambling is slightly greater than the barrier for CO scrambling in **5**. Although the two scrambling processes probably proceed by similar pathways, no experimental data are available to indicate precisely what mechanism applies. Calculations by Harlow, McKinney, and Ittel[10a] suggest that while maintaining the M···H···C interaction the allyl group can rotate 120° (resulting in $P(OCH_{3})_{3}$ site exchange) with barriers to such rotations being similar to those observed experimentally. Alternatively, ligand scrambling can occur through dechelation of the coordinated C–H bond followed by 120° rotation of the ML_{3} fragment of the 16-electron π-allyl species as illustrated for $(\eta^{3}\text{-}C_{6}H_{9})Mn(CO)_{3}$, **5**. Albright has calculated the barrier to
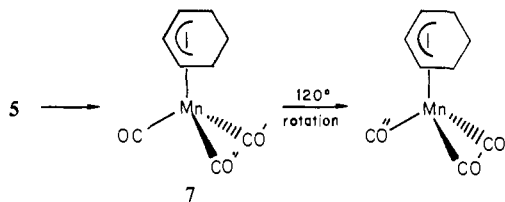
rotation in species **7** as 4.9 kcal/mol.[42] If **7** is close to the transition state for endo C–H bond exchange, then $\Delta G^{\ddagger}$ for the carbonyl-scrambling process should be the sum of $\Delta G^{\ddagger}$ for endo C–H bond exchange (8.3 kcal/mol) and $\Delta G^{\ddagger}$ for π-allyl rotation (4.9 kcal/mol) or 13.2 kcal/mol. This closely matches the experimentally observed $\Delta G^{\ddagger}$ of 13.1 kcal/mol, and we believe this scheme represents a very likely mechanism for the carbonyl-scrambling process.

It is likely that the activation energies for endo C–H exchange ($\Delta G^{\ddagger}$ = 8.3 kcal/mol) and [1,2] metal migration ($\Delta G^{\ddagger}$ = 15.4 kcal/mol) in **5** reflect the relative thermodynamic stabilities of **7** and **8**, the respective intermediates (or transition states) proposed for each process. On the basis of this premise, the 18-electron diene hydride, **8**, appears less stable than the electron-deficient π-allyl species, **7**. Thus, the order of stability in this series appears to be bridged species, **5** (ground state, 18-electron) > π-allyl, **7** (16-electron), > diene hydride, **8** (18-electron), a result not easy to rationalize. Harlow, McKinney and Ittel have performed HMO calculations which explore the relative stabilities of the 18-electron bridged and the 16-electron π-allyl structures in the iron system.[10a] Further calculations which also consider the 18-electron diene hydride structure would be of obvious interest.

As realized earlier by a number of authors,[9b,16] the study of intramolecular M···H···C interactions in transition-metal complexes has potential application to the important area of C–H bond activation. To date, however, most reports have dealt primarily with the structural details of these interactions and few studies have exposed useful chemistry based on this interaction. We have demonstrated that coordination of the C–H bond in **5** and **6** renders the bridging hydrogen acidic, permitting electrophilic

substitution at the α-carbon, a reaction of potential synthetic utility.[17] This effect appears to be characteristic of M···H···C interactions; for example, Schrock has observed enhanced acidity of the bridging hydrogen in electron-deficient tantalum carbene complexes which exhibit substantial M···H···C interactions.[12]

We anticipate that the decreased C–H bond order in these complexes will result in a general enhancement of the reactivity of the coordinated C–H bond toward a variety of reagents. Thus, we are currently exploring the reactions of **5** and its derivatives with reagents other than simple bases with emphasis on identifying reactions of possible synthetic utility.

Experimental Section

All reactions and manipulations were performed under a dry, oxygen-free, nitrogen atmosphere. Tetrahydrofuran solvent was freshly distilled from $LiAlH_{4}$ under a nitrogen atmosphere; other solvents were simply degassed unless otherwise stated.

NMR samples were degassed by several freeze–pump–thaw cycles and NMR tubes were sealed under vacuum (~0.01 mm). Deuterated NMR solvents were dried over molecular sieves (4 Å) and stored under nitrogen in ampules equipped with Teflon stopcocks. ^{1}H NMR spectra were recorded at 100 MHz by using a Varian XL-100 FT NMR spectrometer; ^{13}C NMR spectra were recorded at 62.9 MHz by using a Brüker WM250 FT NMR spectrometer. Probe temperatures were calibrated by measurement of peak separations in standard methanol or ethylene glycol samples. Infrared spectra were recorded on a Beckman spectrophotometer (IR 4250), and frequencies were assigned relative to a polystyrene standard.

(Benzene)manganese tricarbonyl hexafluorophosphate and (cyclohexadienyl-d_{7})manganese tricarbonyl were prepared according to published procedures.[43]

Preparation of Cyclohexenylmanganese Tricarbonyl, 5. (Benzene)-manganese tricarbonyl hexafluorophosphate (5.80 g) was suspended in 100 mL of THF and 50 mL of $LiBEt_{3}H$ (1 M in THF) was added dropwise with stirring. The solid reacts almost immediately resulting in formation of a deep red homogeneous solution. After ca. 30 min of stirring at room temperature, IR analysis of the reaction mixture (CO region) indicates complete conversion to the diene anion.[17] The solution was cooled to 0 °C, and 200 mL of $H_{2}O$ was added slowly with stirring. Triethylamine (7 mL) and petroleum ether (100 mL, bp 35–60 °C) were then added, and the mixture stirred vigorously for ca. 10 min resulting in formation of a red aqueous layer and an orange organic layer. The organic layer was separated, and the aqueous layer was extracted with five additional 100-mL portions of petroleum ether. The organic fractions were combined, dried over anhydrous $Na_{2}SO_{4}$, filtered, and evaporated (25 °C (20 mm)) to a red oil. The oil was chromatographed on a column of basic alumina (activity II) using petroleum ether as eluent. A major yellow band which eluted first was collected and evaporated (25 °C (20 mm)) to a yellow-orange oil (2.59 g), identified as **5** by ^{1}H NMR. This material was purified by dissolution in a minimum amount of petroleum ether and cooling to -78 °C resulting in precipitation of yellow-orange crystals. The solvent was decanted and the product, which melts at 0 °C, was dried under high vacuum (0.01 mm), giving 2.39 g of **5** (68% yield based on $C_{6}H_{6}$ $Mn(CO)_{3}PF_{6}$). Anal.: C, 48.80; H, 4.31; Mn, 25.21.

Preparation of (6-endo-Methylcyclohexenyl)manganese Tricarbonyl, 6b. Potassium hydride (0.28 g) was suspended in 40 mL of THF and 0.357 g of cyclohexenylmanganese tricarbonyl, **5**, was added with stirring at room temperature. The yellow color attributed to **5**, rapidly disappears, giving an almost clear solution of the diene anion, **4** (confirmed by IR). After ca. 30 min the anion solution was filtered through glass wool/celite to remove excess KH. The filtrate was slowly added with stirring to a flask containing 0.65 mL of $CH_{3}I$ (ca. 10-fold excess) causing immediate formation of a white precipitate (KI) and an orange solution. The KI was removed by filtration through glass wool/celite, and the filtrate was evaporated 25 °C (20 mm)) to an orange oil. The oil was extracted with a minimum amount of petroleum ether, filtered through celite to remove residual KI, and evaporated again to an orange oil. Remaining traces of solvent were removed under high vacuum (0.01 mm), giving 0.296 g of monomethylated product, **6** (79% yield based on **5**). In solution this material exists as a 22:78 mixture of the 5-endo-methyl and 6-endo-methyl isomers which are in rapid equilibrium as demonstrated by their temperature dependent ^{1}H NMR spectra.[17] The 6-endo-methyl isomer, **6b**, appears to be less soluble in petroleum ether and can be crystallized selectively from solutions at -20 °C (mp 40–42 °C; recrystallized yield undetermined). The infrared spectrum of this

(42) Albright, T. A., unpublished results.

(43) Lamanna, W.; Brookhart, M. *J. Am. Chem. Soc.* **1980**, *102*, 3490.

material in the carbonyl stretching region was identical with that of the parent complex: ν_{CO}(petroleum ether) 2020 (s), 1945 (s), and 1937 (s) cm^{-1}.

Preparation of Partially Deuterated Cyclohexenylmanganese Tricarbonyl. To a solution of (cyclohexadienyl-d_7)manganese tricarbonyl (0.454 g) in 40 mL of THF was added 4.04 mL of LiBEt$_3$H (1 M in THF) dropwise with stirring. The resulting solution is nearly colorless (light yellow), and IR analysis (CO region) after 30 minutes indicates quantitative formation of the diene anion **4**. The reaction mixture was cooled to 0 °C and ca. 25 mL of D$_2$O (99.7% D) added slowly with stirring. The workup of this material was identical with that used in the preparation of the unlabeled complex **5**. The unrecrystallized product was isolated in quantitative yield (0.462 g); however, upon recrystallization this was reduced to 83%. On the basis of the ^{1}H NMR spectrum, the material isolated is not the expected cyclohexenyl-d_8 complex possessing a single exo or olefinic proton. Instead, a mixture of deuterium-labeled cyclohexenyl products was obtained with various degrees of ^{1}H incorporation into both exo, olefinic, and endo positions. A discussion of the possible origin of this mixture and an analysis of the complex ^{1}H NMR spectra are included in the results section.

X-ray Data Collection. Well-formed orange crystals of [η^3-C$_6$H$_8$-(CH$_3$)]Mn(CO)$_3$, **6b** were precipitated from a petroleum ether solution of **6** at −20 °C. A single crystal approximately 0.25 × 0.25 × 0.45 mm was sealed in a glass capillary under a nitrogen atmosphere. X-ray analysis was carried out on an Enraf-Nonius CAD-4 automated diffractometer using graphite crystal monochromated Mo Kα radiation. The unit cell parameters, obtained from least-squares refinement of 25 accurately centered reflections, are $a = 6.546$ (4) Å, $b = 9.818$ (3) Å, $c = 17.250$ (5) Å, $\beta = 112.00$ (3); and $V = 1028.0$ Å. The calculated density is 1.52 g cm^{-1}. The space group was uniquely determined from systematic absences in $h0l$ for $l = 2n + 1$ and $0k0$ for $k = 2n + 1$ to be $P2_1/c$ [C_{2h}^5, No. 14].

Data were collected by a ω–2θ scan technique (ISCANT = 5) with a takeoff angle of 2.6°. The scan rate was variable and determined by a fast (7° min^{-1}) prescan. Slow scans were performed on reflections with prescan intensity $\geq 1\sigma$. Calculated speeds based on the net intensity gathered in the prescan ranged from 7 to 0.8° min^{-1}. Moving-crystal moving-counter backgrounds were collected for 25% of the total scan width at each end of the scan range. For each intensity the scan width was determined by the equation

$$\text{scan range} = A + B \tan \theta$$

where $A = 0.80°$ and $B = 0.35°$. Aperture settings were determined in a like manner with $A = 1.25$ mm and $B = 1.00$ mm. As a check on the stability of the crystal, three reflections were chosen as intensity standards and were measured after every three hours of X-ray exposure time. Two reflections were chosen as reflection standards and were measured every 200 reflections. The standards fluctuated within a range of ±2%.

One independent octant of data was measured out to $2\theta = 55°$, and a slow scan was performed on a total of 2577 unique reflections. Of these, 1652 had intensity greater than 3σ, were considered observed, and were used in subsequent structure solution and refinement. The intensities were corrected for Lorentz–polarization effects.

Structure Solution and Refinement. The solution and refinement of the structure was carried out on a PDP-11 computer using programs supplied by Enraf-Nonius.[44] Atomic scattering factors were taken from Cromer and Waber,[45] and in least-squares refinement the function $\sum w$-$(|F_o| - |F_c|)^2$ was minimized. The standard deviations of the observed structure factors were based on counting statistics with a correction factor, p, of 0.01. With use of this value, R_w showed little dependence on intensity which indicated that this was a correct weighing scheme.

The position of the manganese atom was deduced from a Patterson map and subsequent calculation of difference Fourier maps allowed the location of other nonhydrogen atoms. Refinement using isotropic temperature factors led to $R = \sum ||F_o| - |F_c||/\sum |F_o| = 0.101$ and $R_w = [\sum w(|F_o| - |F_c|)^2/\sum w|F_o|^2]^{1/2} = 0.103$. Conversion to anisotropic temperature factors and further refinement led to $R = 0.061$ and $R_w = 0.072$. The hydrogen atoms, including the bridging hydrogen, were easily located on a difference Fourier map, and both their positional and isotropic thermal parameters were refined. A final least-squares refinement yielded $R = 0.042$ and $R_w = 0.041$.

A final difference Fourier map showed no feature greater than 0.3 e Å^{-3}. The estimated standard deviation of an observation of unit weight was 2.4. The final data to parameter ratio was 9.7:1.

Supplementary Material Available: A listing of structure factors for **6b** (12 pages). Ordering information is given on any current masthead page.

(44) All programs used for structure solution and refinement were part of the Structure Determination Package (SDP) provided by B. Frenz through Enraf-Nonius.

(45) Cromer, D. T.; Waber, J. T. "International Tables for X-ray Crystallography"; Ibers, J. A., Hamilton, W. C., Kynoch Press: Birmingham, England, 1974; Vol. IV, Table 2.2A.